Onset and evolution of Kīlauea’s 2018 flank eruption and summit collapse from continuous gravity

Michael Poland*
U.S. Geological Survey – Cascades Volcano Observatory, 1300 SE Cardinal Ct., Suite 100, Vancouver, WA 98660, USA, Tel.: +1 360-993-8906, Email: mpoland@usgs.gov

Daniele Carbone
Istituto Nazionale di Geofisica e Vulcanologia, Sezione di Catania, Osservatorio Etneo, Catania 95125, Italy

Matthew R. Patrick
U.S. Geological Survey – Hawaiian Volcano Observatory, 1266 Kamehameha Ave, Suite A8, Hilo, HI 96720, USA

*corresponding author

Highlights:

- Gravity changes accompanying the withdrawal of lava lakes from the summit and Puʻu ʻŌʻō vents at Kīlauea Volcano, Hawaiʻi, are the largest ever recorded by continuous monitoring.
- Densities of both lava lakes were < 2000 kg/m^3, and the Puʻu ʻŌʻō lava column was denser than that of the summit.
- A gravity transient at Puʻu ʻŌʻō preceded the onset of the lower East Rift Zone dike intrusion in 2018, possibly related to a small fissure eruption—the first event of the 2018 activity.

Abstract

Prior to the 2018 lower East Rift Zone (ERZ) eruption and summit collapse of Kīlauea Volcano, Hawaiʻi—the most significant eruptive activity at the volcano in 200 years—continuous gravimeters operated on the vent rims of ongoing eruptions at both the summit and Puʻu ʻŌʻō. These instruments captured the onset of the 2018 lower ERZ eruption and the effects of lava withdrawal from both locales, providing constraints on the timing and style of activity and the physical properties of the lava lakes at both locations. At the summit, combining gravity, lava level, and a three-dimensional model of the vent indicates that the upper ~200 m of the lava lake had a density of about 1700 kg m^{-3}, slightly greater than estimates from 2011–2015 and possibly indicating a gradual densification over time. At Puʻu ʻŌʻō, gravity and vent geometry were used to model both the density and the rate of crater collapse, which was unknown owing to a lack of visual observations. Results suggest the withdrawal of at least 11 x 10^6 m^3 of lava over the course of two hours, and a material density of 1800–1900 kg m^{-3}. In addition, gravity data at Puʻu ʻŌʻō captured a transient decrease and increase about an hour prior to crater collapse and that was probably related to a small, short-lived fissure eruption on the west flank of the cone and possibly to dike intrusion beneath Puʻu ʻŌʻō. The fissure was the first event in the subsequent cascade that ultimately led to the extrusion of over 1 km^3 of lava from lower ERZ vents, collapse of the summit caldera floor by more than 500 m, and the destruction of over 700 homes and other structures. These results emphasize the importance of continuous gravity in operational monitoring of active volcanoes.

Keywords: gravity change; Kīlauea Volcano; volcano monitoring; lava lake; fissure eruption; lava density

1.0 Introduction

The 2018 flank lava effusion and summit collapse at Kīlauea Volcano was the most significant volcanic event to have occurred in Hawaiʻi for at least 200 years (Neal et al., 2019). Prior to the event, Kīlauea hosted two long-lived eruptions (Figure 1). Since 1983, Puʻu ʻŌʻō and nearby vents on the volcano's East Rift Zone (ERZ), about 20 km downrift of the summit, erupted approximately 4.4 km^3 of lava over 35 years (Neal et al., 2019). Starting in 2008, a second eruptive vent, which hosted a lava lake, was active within Halema‘uma‘u crater at the volcano's summit (Patrick et al., 2019a). Both of these eruptions came to an end with the onset of a magmatic intrusion on April 30, 2018, that migrated to the lower ERZ over the ensuing days. The intrusion occurred after a weeks-long buildup in pressure at both Pu‘u ‘Ō‘ō and the summit, manifested by rising lava levels and inflationary deformation (Patrick et al., 2020), which are typical precursors before changes in eruption patterns at Kīlauea (e.g., Lundgren et al., 2013; Patrick et al., 2015, 2019a; Poland et al., 2016). The crater floor at Pu‘u ‘Ō‘ō collapsed on April 30 as magma beneath the cone drained in response to the intrusion; at the volcano's summit 20 km uprift from Pu‘u ‘Ō‘ō, subsidence and lava lake withdrawal began a day later (Anderson et al., 2019). The lower ERZ eruption commenced within the Leilani Estates subdivision, about 40 km from the summit (20 km downrift from Pu‘u ‘Ō‘ō), on May 3 with the eruption of cool, relict lava that had been stored in the lower ERZ for decades (Gansecki et al., 2019). On May 4, a M6.9 earthquake occurred on Kīlauea's south flank, probably caused by stress imposed by the ERZ intrusion (Neal et al., 2019; Kundu et al., 2020; Patrick et al., 2020). Lower ERZ eruptive activity intensified in mid and especially late May, with the eruption of hotter, more fluid, and less chemically evolved magma derived from the summit reservoir complex; this activity occurred from the vent designated Fissure 8 (Gansecki et al., 2019). Subsidence of Kīlauea's summit caldera took place throughout the eruption, evolving from steady sagging to a series of near-daily several-meter downdropping events, accompanied by M_w5.2–5.4 earthquakes and interspersed with subsidence (Anderson et al., 2019; Neal et al., 2019; Segall et al., 2019, 2020). These impulsive collapses were related to effusive pulses from the lower ERZ vent (Patrick et al., 2019c). Significant lava effusion stopped abruptly on August 4, after the eruption of 0.9-1.4 km^3 of lava (Dietterich et al., in review). Summit collapse ended at the same time, with a maximum downdrop of more than 500 meters (Neal et al., 2019).

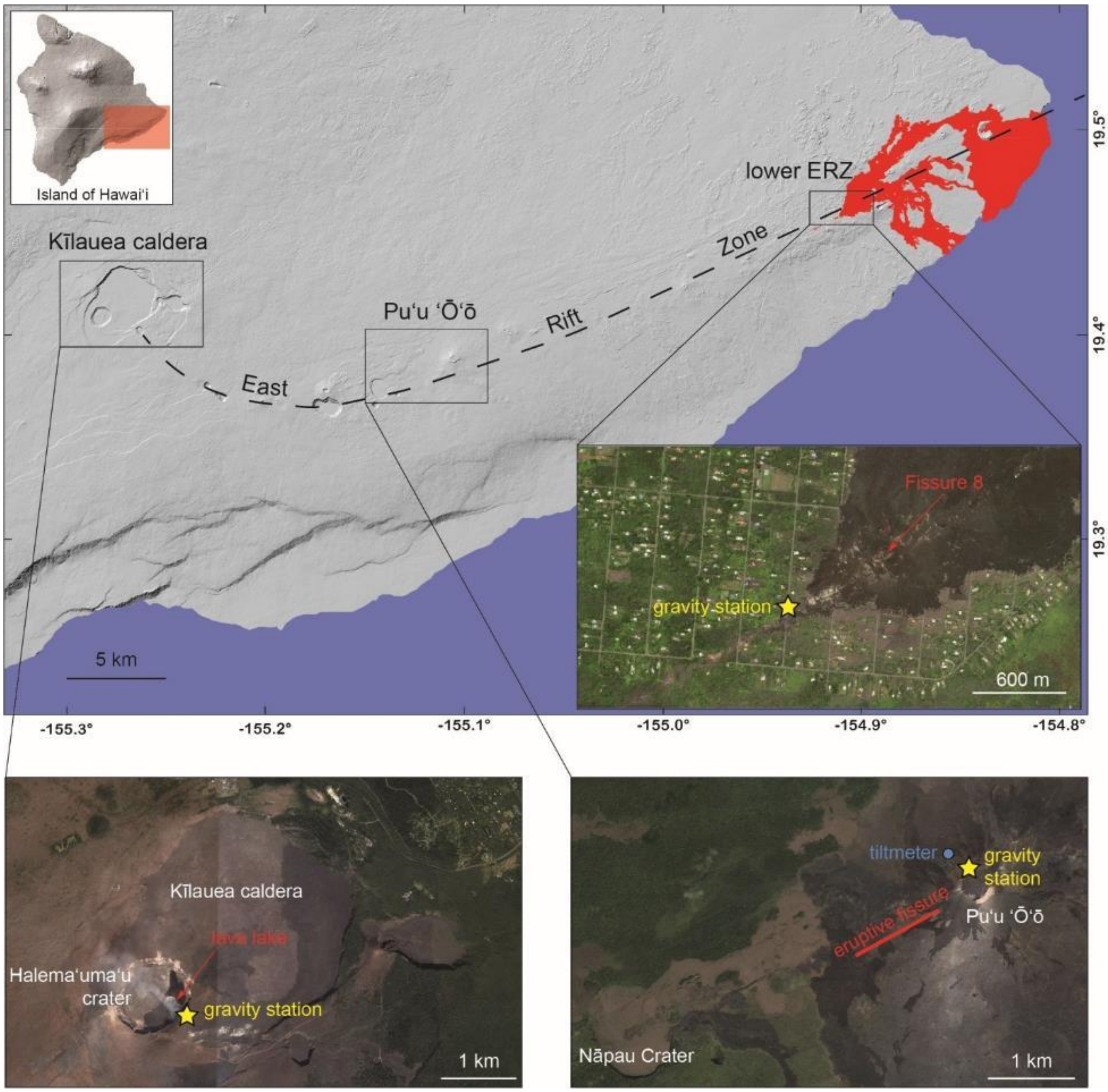

Figure 1. Location map showing the summit caldera and East Rift Zone (ERZ) of Kīlauea Volcano, Hawai'i. Red area on the map shows 2018 lower ERZ lava flows. Zoomed areas show the locations of (i) continuous gravity stations (yellow stars) at the summit and Pu'u 'Ō'ō eruptive vents, (ii) the tiltmeter at Pu'u 'Ō'ō (blue circle), and (iii) the temporary station deployed on 3 separate occasions near the lower East Rift Zone (ERZ) Fissure 8 eruptive vent. Collocated with the gravity stations at the summit and Pu'u 'Ō'ō were GNSS stations and visible/thermal cameras.

Kīlauea's 2018 eruptive sequence was preceded by weeks of pressurization of the magmatic system, detected by deformation monitoring at the summit, along the middle ERZ, and at Pu'u

‘Ō‘ō, so Kīlauea was clearly “primed” for an eruption (Patrick et al., 2020). Details of the onset of this major eruptive event, however, are uncertain. Field inspection of Pu‘u ‘Ō‘ō on May 1 revealed the presence of a ~1-km-long fissure on the west flank of the cone (Figure 2), with a small amount of lava having erupted from the upper (eastern) third of the fissure but the timing and significance of this feature were unclear (Neal et al., 2019). Fortunately, Kīlauea hosts a continuous gravity monitoring network—one of very few such networks worldwide. Measurement of change in gravity over time, also called microgravity, offers a window into subsurface mass transport due to, for example, magma storage and migration. At Kīlauea, continuous gravimeters were operational at both Pu‘u ‘Ō‘ō and the summit prior to and during the 2018 lower ERZ eruption and summit collapse. These data provide insights into the crucial first minutes of the initial changes at Pu‘u ‘Ō‘ō that preceded the formation of the lower ERZ intrusion and also constrain the physical properties of the lava lakes at the summit and Pu‘u ‘Ō‘ō.

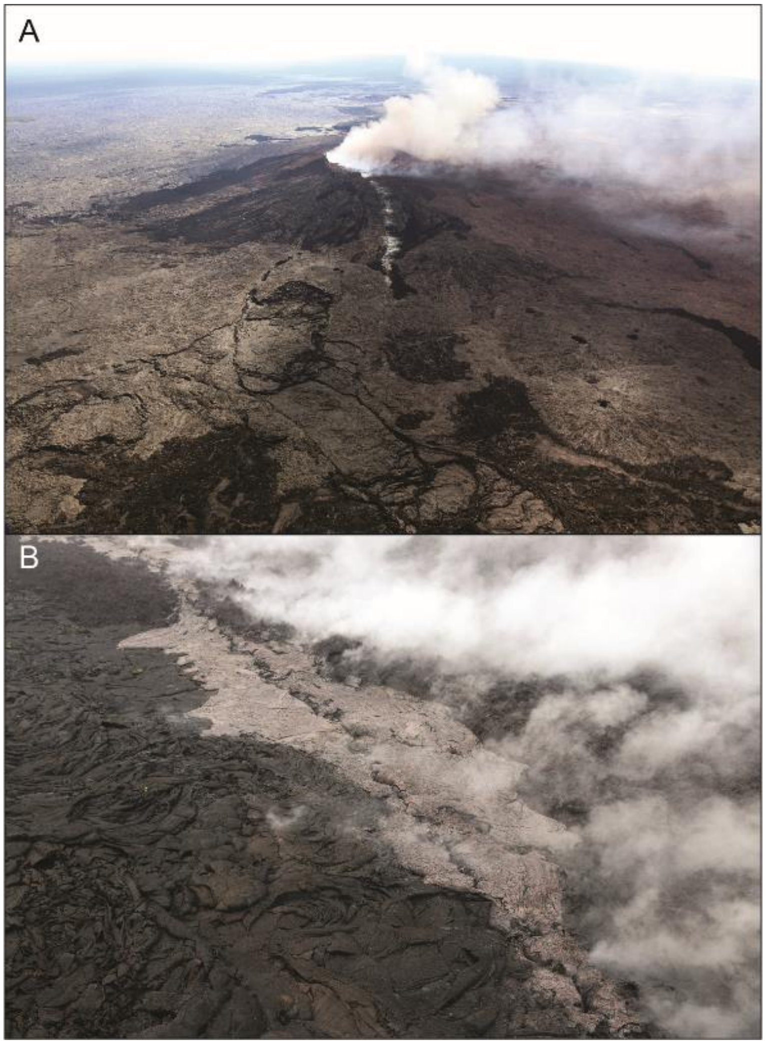

Figure 2. Photos of the eruptive fissure on the west flank of Puʻu ʻŌʻō cone. Location of the fissure is given in the zoomed view of Puʻu ʻŌʻō in Figure 1. (A) Aerial view of the eruptive fissure looking east. USGS photo from May 3, 2018. (B) Close-up aerial view of a segment of the eruptive fissure and minor degassed lava flows. USGS photo from May 1, 2018.

2.0 Data and Methods

At the end of April 2018, continuous gravimeters were functioning on the rims of both the summit and Puʻu ʻŌʻō eruptive vents at Kīlauea, collocated with continuous GPS stations and visible and thermal cameras (Figure 1). The summit cameras, along with a laser rangefinder, allowed for detailed tracking of the lava level over time (Patrick et al., 2019a,b). At Puʻu ʻŌʻō, the camera view and frame rate were sufficient for seeing the crater floor and determining the timing of the onset of collapse, but it was not able to track the collapse over time, since the crater floor quickly dropped out of view. GPS stations at both locations provided vertical displacement over time, which was needed to determine the contribution of elevation change to the gravity signal, and tiltmeters helped to provide higher temporal resolution for determining changes in deformation rate and style. Following drainage of the summit lava lake and collapse of the crater floor at Puʻu ʻŌʻō by early May 2018, overlapping aerial photos provided data needed to develop Structure-from-Motion (SfM) models of the crater interiors--data that were used to model the gravity changes in both locations.

2.1 Gravity

Both the summit and Puʻu ʻŌʻō gravimeters were LaCoste and Romberg G-model instruments upgraded with electronic feedback systems and outputting gravity, temperature, voltage, long level, and cross level at 2 Hz (Carbone et al., 2013; Poland and Carbone 2016, 2018). The summit gravimeter, HOVL-G, was installed in 2010 (Carbone and Poland, 2012) and operated with few gaps until January 2016, when it went offline owing to mechanical issues (in August of that year, the power system was destroyed by a small explosive event from the summit vent). The instrument was revived in early 2018 and operated until May 15, when it was consumed by the widening and collapse of Halemaʻumaʻu crater. The Puʻu ʻŌʻō gravimeter, PUOC-G, was installed in 2012 and operated through late 2016 before suffering a mechanical failure. It was repaired and reinstalled in mid-April 2018, in time to track the gravity signature of the rapid deformation of Puʻu ʻŌʻō, which started in March of that year (Patrick et al., 2020), and it operated continuously until it was removed on June 7, 2018. Gravity data are provided in Poland (2020).

We adjusted the gravity data for Earth tides using the ETERNA software (Wenzel, 1996). The effect of elevation changes was evaluated using vertical deformation from collocated GPS stations and assuming a Bouguer-corrected free-air gradient (derived via procedure in Carbone et al., 2013) of -236 μGal/m. For both HOVL-G and PUOC-G, the free-air correction is a small fraction—less than 5%—of the total measured gravity change during the onset and evolution of the 2018 activity.

2.2 Structure-from-Motion point clouds

We constructed three-dimensional surface models of the drained summit and Puʻu ʻŌʻō eruptive vents using structure-from-motion (SfM) processing of overlapping aerial images collected using a handheld thermal camera (Patrick et al. 2019a). Helicopter overflights of the summit eruptive vent occurred on May 8 and 9, 2018, and at Puʻu ʻŌʻō on May 11. Images were processed using Agisoft Photoscan. The summit point cloud was georeferenced using identifiable points on the rim of the eruptive vent and the summit, the horizontal coordinates of which were taken from WorldView satellite images and with elevations from a 5 m DEM acquired in 2005. At Puʻu ʻŌʻō, kinematic GPS positions of features that were identifiable in the thermal images were used to georeference the point cloud. Point-cloud data of the summit eruptive vent are available from Patrick et al. (2019b). For Puʻu ʻŌʻō, the point cloud data are given by Patrick (2020).

3.0 Summit gravity change

At the summit gravity station, HOVL-G (Figure 1), strong gravity changes were recorded between 30 April and 7 May 2018 (Figure 3a). During a 10-hour period on 30 April and 1 May, a ~100 μGal gravity increase occurred even though the dike had begun propagating from Puʻu ʻŌʻō towards the lower ERZ during this time. The increase is a result of lava level rise associated with the inflation phase of a DI (deflation-inflation) event (Anderson et al., 2015) that was ongoing at the time. Lava level and gravity then stabilized until 2 May, when the lava level began to recede (Figure 3b), leading to a gravity decrease of more than 1000 μGal over the ensuing 5 days as the lava level dropped by ~200 m.

Given the correspondence of gravity and lava level, the observed gravity changes probably reflect mass changes in the uppermost part of the eruptive vent as lava level rose and fell. Changes in groundwater levels can also cause gravity variations, but studies of gravity change at Kīlauea discount this as a significant contributing factor due to the ~500 m depth of the water table—well below the lava level—and minor observed variations in water levels during previous time periods (e.g., Johnson et al., 2010; Bagnardi et al., 2014; Poland and Carbone, 2016).

Water table variations are especially unlikely to contribute to 2018 gravity changes given the short timescale and large magnitude of the signal (Figure 3a). Carbone et al. (2013) and Poland and Carbone (2016) explored the correspondence between gravity and lava level for previous episodes of lava lake fluctuation and gravity change by developing a numerical model of the eruptive vent based on visual observations and lidar data. This model was used to calculate the density of the lava given the lava level changes determined from thermal camera data and the gravity change. They found that during a 2011 draining of the summit lava lake, the upper 120 m of the lake had a density of 950 ± 300 kg m^{-3} (Carbone et al., 2013), and over the course of 2011–2015, the density remained in the range of 1000–1500 kg m^{-3} (Poland and Carbone, 2018).

We followed a similar approach for assessing the density of the upper 200 m of the lava lake during the May 2–7, 2018, draining, utilizing the SfM point-cloud data to develop a model of the eruptive vent that accounts for even second-order features of vent geometry (Figure 4). The model of the vent was created as an array of 5x5 m cells (square-based vertical parallelepipeds) whose bottom elevations are obtained from the point-cloud data. At a given time, the observed level of the lava lake constrains the cells that are "active" and those that are excluded from the calculation of the gravity effect based on the lava level, and also the top-to-bottom elevation difference—in other words, the volume of lava within the vent. Although the gravity data were adjusted for Earth tides and the Bouguer-corrected free-air gradient (based on the vertical deformation at the collocated GPS station; Figure 3c), there is still an unknown amount of instrumental drift, which is a problem when examining any gravity records from spring devices, that span more than a few days (Poland and Carbone, 2016). We assume that this drift is linear (Carbone et al., 2017) and utilize an optimization procedure that automatically finds the values of drift rate and lava density by minimizing the misfit between observed and modeled gravity change, given the lava level fluctuation (after both time series are resampled to 1 hour intervals; Figure 3d). The optimal values of lava density and instrumental drift are 1700 kg m^{-3} and 30 µGal/day, respectively; the RMS error between observed and calculated gravity changes is 14 µGal. Through the SfM model of the vent and the observed lava level change, it is possible to precisely estimate the volume of material lost from the vent during the May 2–7 draining: 9 x 10^6 m^3. Assuming that the low-density value of 1700 kg m^{-3} is due to the presence of exsolved gas (bubbles) in the lava lake, the above volume corresponds to ~6 x 10^6 m^3 of dense-rock-equivalent magma (DRE).

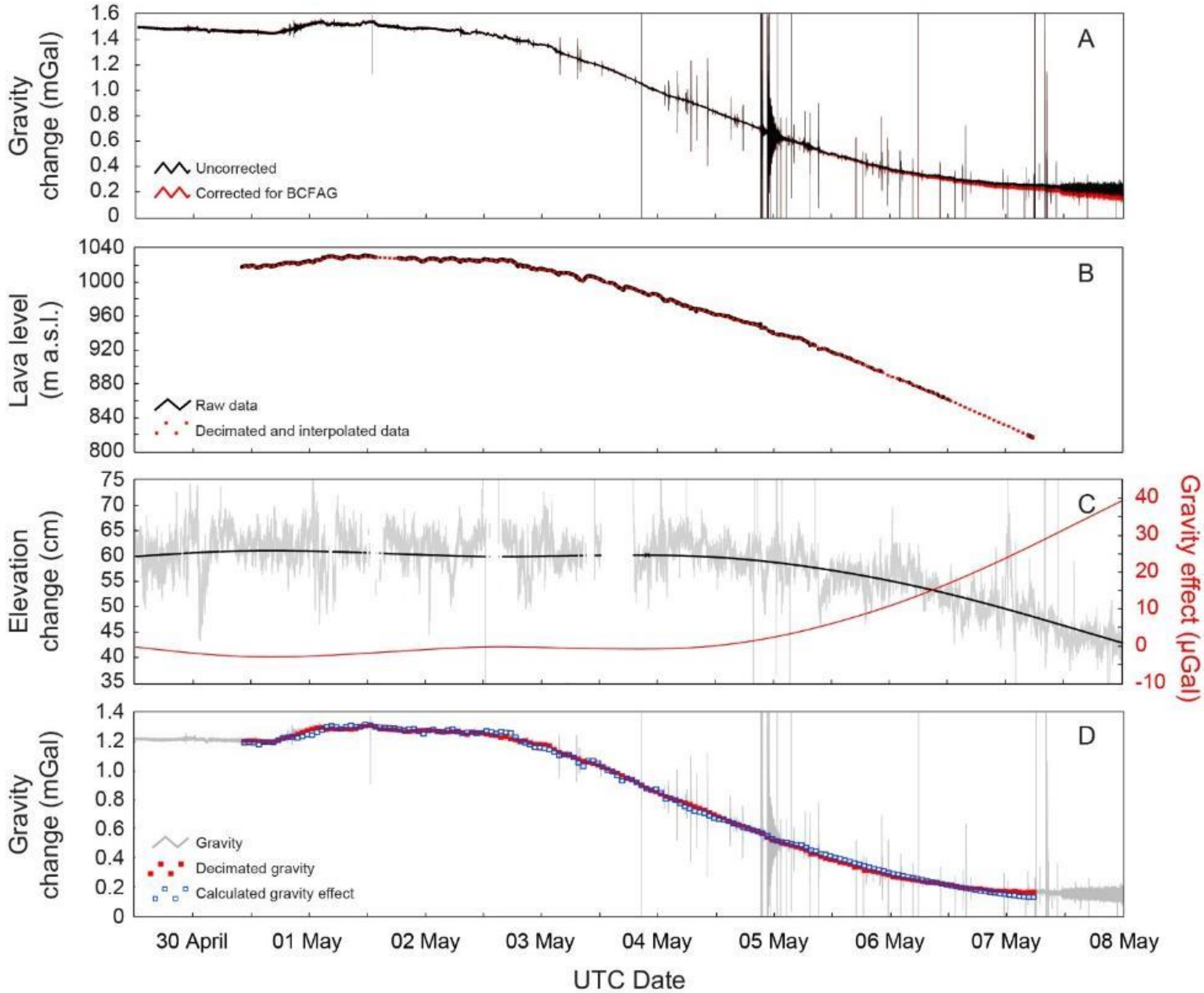

Figure 3. Summit gravity, deformation, and lava-lake level changes during April 30 - May 8 (UTC). (A) Gravity change from summit instrument. Black line is gravity change after correction for Earth tides. Red line is gravity change also adjusted for the Bouguer-corrected free-air gradient (BCFAG). (B) Lava level in the summit vent, from Patrick et al. (2019b). Red dots are decimated and interpolated data. (C) Elevation change from GPS station collocated with gravimeter. Gray line is raw high-rate data, and back line is smoothed displacement. Red line is the gravity effect of the vertical deformation, assuming a Bouguer-corrected free-air gradient of -236 µGal/m. (D) Decimated (red) and modeled (blue) gravity change overlain on gravity signal corrected for tide and vertical deformation (gray).

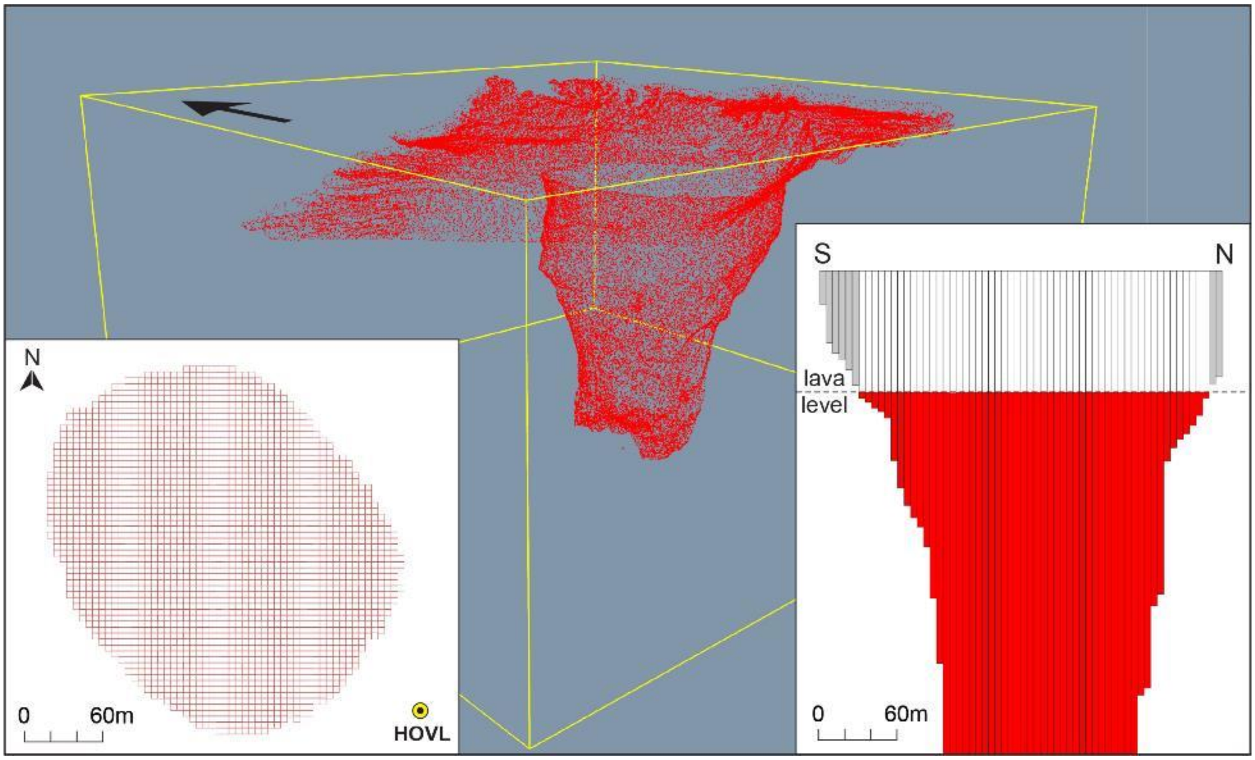

Figure 4. Point cloud assembled using Structure from Motion and oblique airborne thermal imagery of the summit eruptive vent following withdrawal of the lava lake. Arrow indicates north direction. Insets show plan view (lower left, with yellow circle indicating the location of the summit gravimeter) and north-south cross section (lower right) of the model used to approximate gravity change due to variations in lava level.

4.0 Puʻu ʻŌʻō gravity change

Gravity change at Puʻu ʻŌʻō was greater in magnitude and occurred over a shorter time period compared to summit gravity change (Figure 5a). Starting at about 14:15 on April 30 HST (00:15 UTC on May 1), gravity began to decrease, dropping by over 200 µGal in 8 minutes. Gravity then increased by almost 400 µGal in the subsequent 10 minutes and remained mostly stable until about 15:15 HST (01:15 UTC), when a precipitous drop began. Over the course of the ensuing 1.5 hours, gravity decreased by about 1500 µGal before stabilizing. This gravity drop did not occur at a constant rate; about 60% of the change occurred between 15:30 and 16:00 HST (01:30 and 2:00 UTC). We believe that this complex pattern reflects two signals: a brief fissure eruption on the west flank of Puʻu ʻŌʻō (Figure 2) followed less than an hour later by withdrawal of magma from beneath Puʻu ʻŌʻō in response to the intrusion that had begun moving downrift onwards the lower ERZ.

4.1 Gravity change due to collapse of the crater floor

The ~1500 µGal gravity drop that occurred at Puʻu ʻŌʻō on April 30 between 15:15 and 16:45 HST (May 1 between 01:15 and 02:45 UTC; Figure 5A) is by far the largest gravity change ever recorded at any volcano by continuous measurements, both in terms of total magnitude and rate. The gravity change was a result of magma withdrawal from beneath Puʻu ʻŌʻō, which removed support from, and caused collapse of, the crater floor. This interpretation is consistent with tilt data (Figure 5B) from a site about 250 m northwest of the gravimeter (Figure 1) and with webcam imagery of Puʻu ʻŌʻō crater. Although weather was poor, the unmistakable onset of collapse of the crater floor at Puʻu ʻŌʻō was indicated by a thermal webcam image acquired at 15:25 HST on April 30 (01:25 May 1 UTC). Subsidence of the crater floor may have been occurring before this time but was small compared to the collapse itself. The crater floor dropped quickly out of view of the webcams, and by shortly after 16:00 HST (02:00 UTC) the cameras were obscured by ash generated by the collapse.

At about the same time that crater floor collapse was clear in webcam imagery there was a change in tilt direction, from west- to east-directed tilt (Figure 5B). The north component of tilt, which had gone off-scale due to large pre-collapse north-directed tilt (see section 4.2), came back on scale just after 16:00 HST (02:00 UTC), indicating that north-directed tilt had switched to south-directed tilt at some point—probably at the same time as the change from west- to east-directed tilt. Tilt to the southeast is consistent with withdrawal of lava from Puʻu ʻŌʻō crater. The east component of tilt went off scale shortly after 16:00 HST (02:00 UTC)—a sign of the huge magnitude of the tilt changes.

The gravity decrease associated with collapse of Puʻu ʻŌʻō crater occurred in three phases (Figure 5A). The drop accelerated from onset through about 16:00 HST (02:00 UTC), accumulating about 980 µGal over 45 minutes. The gravity decrease then slowed, with about 160 µGal occurring over the ensuing 20 minutes before accelerating again, with a gravity decrease of about 330 µGal during

16:20–16:45 HST (02:00–02:45 UTC). These changes in rate presumably reflect an uneven rate of magma withdrawal from beneath the crater, although this cannot be confirmed. Seismic tremor remained elevated throughout the collapse, with no obvious correlation to the changes in the rate of gravity decrease. There were also no obvious correlations between ground tilt and the rate of gravity decrease, but at least one component of the tiltmeter was off scale during all parts of the collapse (Figure 5B).

Because there is no record of the rate of withdrawal from webcam imagery, it is not possible to constrain the density of the material that drained from beneath Puʻu ʻŌʻō via matching the gravity and lava level changes, as was done for the summit (see Section 3.0). However, the rate of collapse can be estimated as part of the density calculation, given knowledge of the level of the crater before and after collapse, and a SfM model of the vent geometry obtained from photos taken via a post-collapse helicopter overflight (Figure 6). Before collapse, the elevation of the crater floor at Puʻu ʻŌʻō was estimated to be 850 m. After the collapse, the crater bottom, which was composed of rubble from the crater floor and walls, was at about 500 m elevation. This indicates a minimum bulk volume loss of 11 x 10^6 m^3 during 15:00-17:00 HST on April 30 (01:00-03:00 UTC on May 1), given our SfM vent model. The value is a minimum because some rubble infill undoubtedly accumulated between the withdrawal and the May 11 overflight that acquired the images used to create the SfM model. The crater was presumably deeper upon collapse, but the exact depth cannot be known. This complicates calculation of the density of the magma that withdrew from beneath the crater—both a starting and ending depth are required by the model because there is no record of the rate of crater collapse. Nevertheless, we are able to determine a maximum bound on the density by using the crater depth as observed on May 11.

Assuming that the magma level within Puʻu ʻŌʻō decreased from an elevation of 850 m to 500 m during 15:15–16:45 HST (01:15–02:45 UTC), we can estimate the magma density needed to induce the corresponding gravity decrease. We again utilize gravity data corrected for the effects of Earth tides and elevation changes (Figure 5C). The instrumental drift is neglected in this case, since our focus is on gravity change that occurs over a very short interval (~ 2 hours), and the corresponding drift effect is most likely within a few µGal—three orders of magnitude lower than the observed signal.

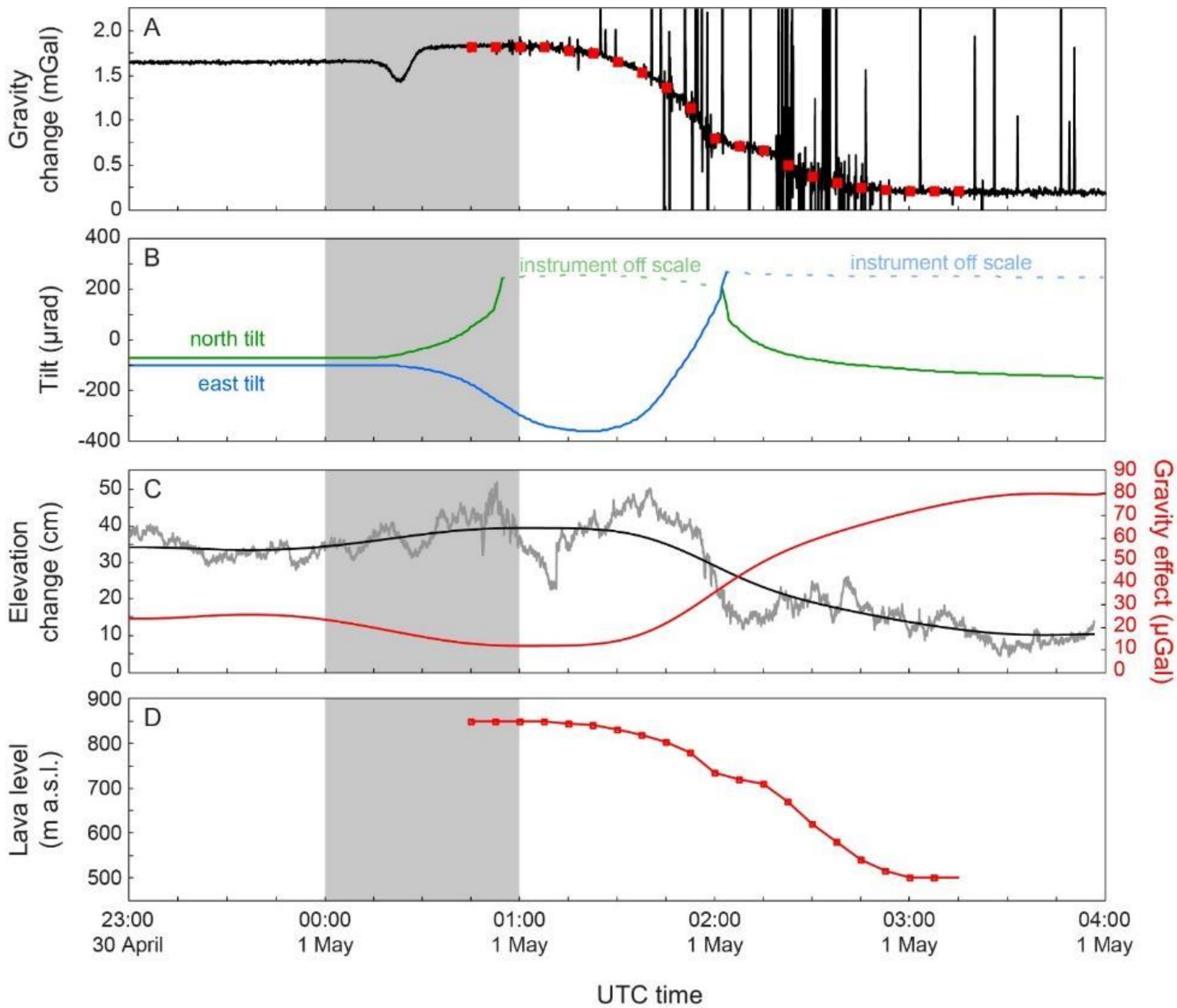

Figure 5. Pu'u 'Ō'ō gravity, deformation, and modeled lava level changes during 23:00 April 30 - 04:00 May 1 (UTC). (A) Gravity change from Pu'u 'Ō'ō instrument. Black line is gravity change after correction for Earth tides. Red dots represent the calculated gravity effect due to the lava level changes in (c), assuming a density of the material that drained from the vent of 1900 kg m^{-3}.. (B) North and east tilt from a tiltmeter located on the north flank of Pu'u 'Ō'ō (Figure 1). Positive change is tilt in the direction indicated. Both tilt components went off scale at various times (indicated by faded dashed line). (C) Elevation change from GPS station collocated with gravimeter. Gray line is raw high-rate data, and back line is smoothed displacement. Red line is the gravity effect of the vertical deformation, assuming a Bouguer-corrected free-air gradient of -236 μGal/m. (C) Modeled lava level change in Pu'u 'Ō'ō crater calculated from decimated gravity data. Gray shading covers time shown in Figure 7.

Assuming that the magma level within Puʻu ʻŌʻō decreased from an elevation of 850 m to 500 m during 15:15–16:45 HST (01:15–02:45 UTC), we calculate a maximum density of about 1900 kg m^{-3} to explain the gravity drop associated with the collapse of the crater floor at Puʻu ʻŌʻō. To test the effect of a greater depth of collapse, we also performed the calculation using an ending elevation of 350 m, obtaining a density of 1800 kg m^{-3}. This minor variation indicates that the ultimate depth of withdrawal has a weak control on the modeled density, which reflects the importance of the distance between the observation and the changing mass (the strength of the gravity change depends on the square of the distance).

Using the maximum density of 1900 kg m^{-3}, we calculate, over time windows of 450 s between 14:45 and 17:15 HST on April 30 (00:45 and 03:15 UTC on May 1), the lava level needed to induce the gravity change that best fits the observed signal (Figure 5D). As expected given the sensitivity to distance, the modeled lava level change has a different pattern than the gravity signal, with a lower drop rate during 15:50-16:00 HST (01:30-2:00 UTC) and higher during 16:15-17:00 HST (2:15-3:00 UTC). This is again due to the fact that level changes in the shallower part of the vent induce stronger gravity changes due to the shorter distance between changing mass and observation point. The farther the changing mass is from the gravimeter, the greater the mass change needed to generate a signal. Under the assumption that the relatively low value of density we estimate is due to the presence of exsolved gas in the vent, the minimum volume loss of 11 x 10^6 m^3 corresponds to ~8 x 10^6 m^3 of magma (DRE) drained from the Pu`u `Ō`ō vent in 2 hours.

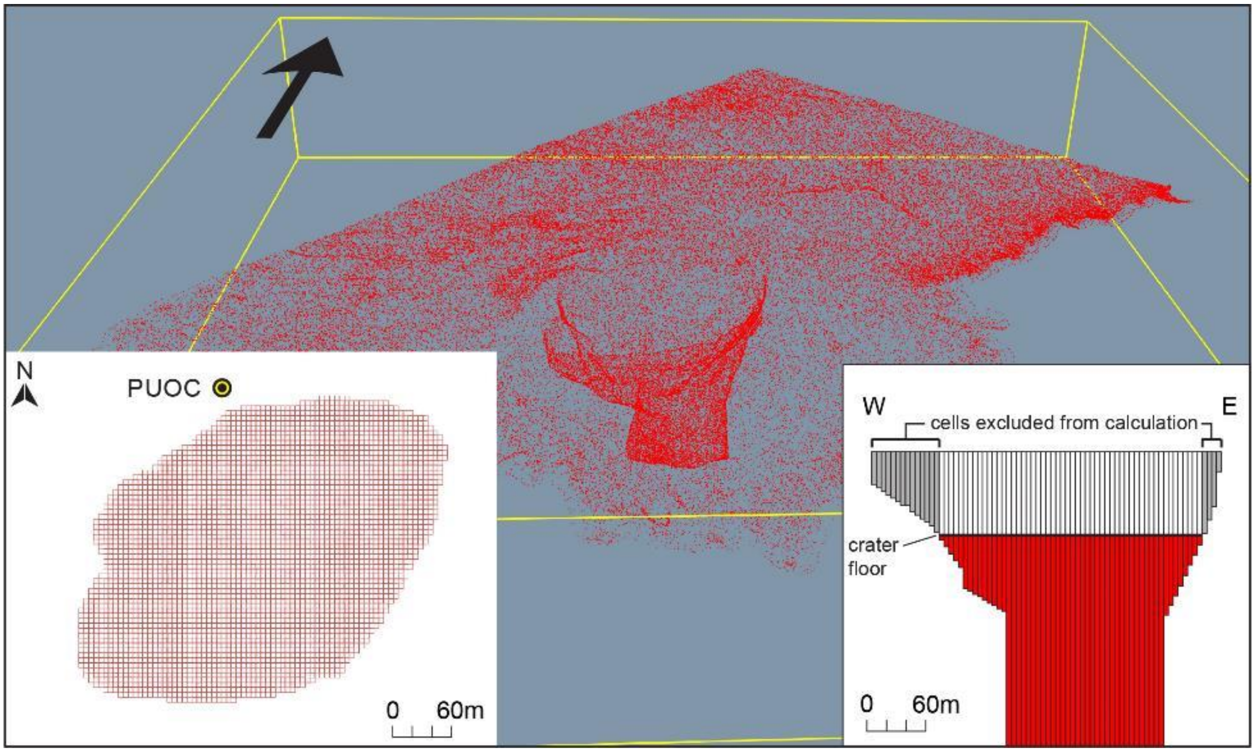

Figure 6. Point cloud assembled using Structure from Motion and oblique airborne thermal imagery of the Puʻu ʻŌʻō eruptive vent following its crater collapse. Arrow indicates north direction. Insets show plan view (lower left, with yellow circle indicating the location of the summit gravimeter) and cross section (lower right) of the model used to approximate gravity change due to variations in lava level.

4.2 Pre-collapse gravity fluctuation

Starting at about 14:12 HST on April 30 (00:12 UTC on May 1), about an hour prior to the onset of collapse of Puʻu ʻŌʻō, northwest-directed tilt was recorded at the tiltmeter on the north flank of Puʻu ʻŌʻō. At about the same time, gravity began to decrease, accumulating approximately 200 µGal in 8 minutes. The gravity drop then reversed, increasing by about 400 µGal over the ensuing 10 minutes. Despite the variation in the sign of gravity change, the tilt direction remained constant (Figure 7), although steadily increasing in rate. The north tilt component went off scale at about 14:55 HST (00:55 UTC). Northwest-directed tilt persisted until about 15:25 HST (01:25 UTC), when the onset of crater-floor collapse became the dominant source of deformation and gravity signal (see section 4.1).

We speculate that the pre-collapse gravity and tilt signals were associated with formation of a ~1-km-long eruptive fissure on the west flank of Puʻu ʻŌʻō—a feature identified during a helicopter overflight on May 1, a day after collapse of the crater floor (Figure 2). There is unfortunately no direct observational evidence for the time of fissure formation, and no discrete seismicity was recorded at the site of the fissure (although a general increase in seismic tremor was recorded by nearby seismometers at the same time as the northwest-directed tilt onset). The northwest-directed tilt, however, is consistent with a pressure source in the vicinity of Puʻu ʻŌʻō—probably the source that resulted in the formation of the eruptive fissure. The tilt and gravity change suggest that the fissure formed in the hour prior to withdrawal of magma from beneath Puʻu ʻŌʻō and was, therefore, the first significant event of the 2018 eruptive sequence.

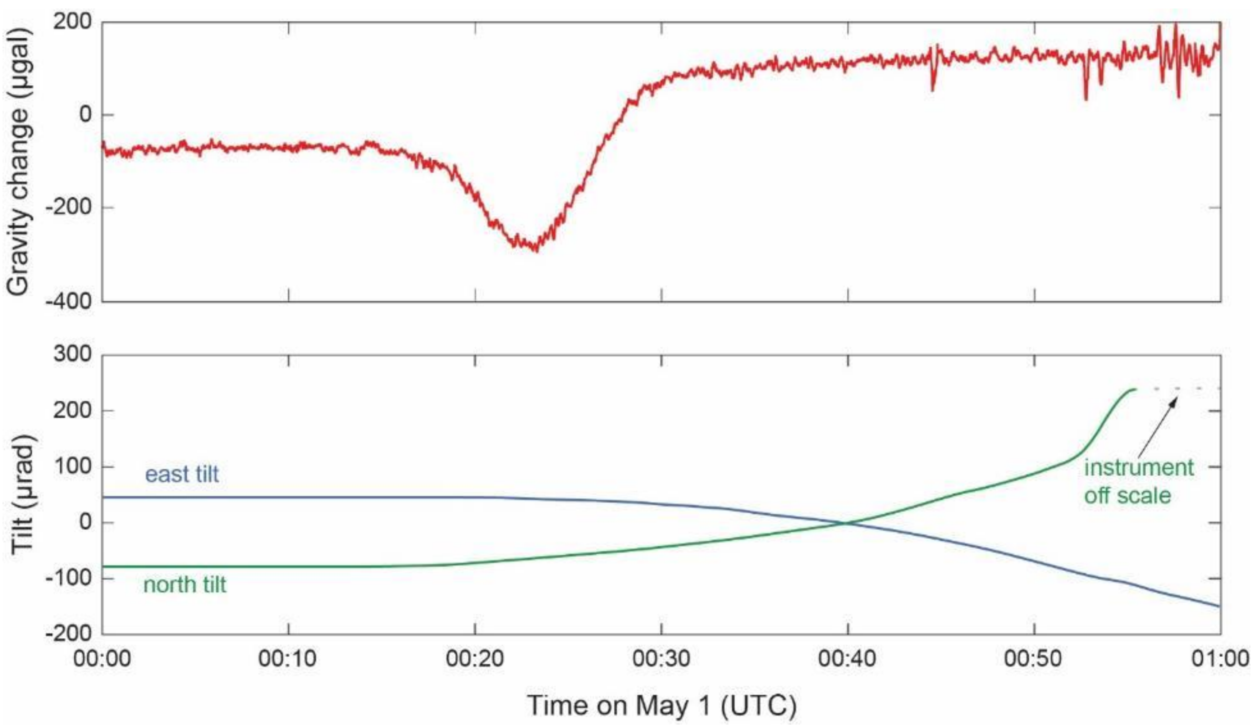

Figure 7. Gravity (top) and ground tilt (bottom) measured at Puʻu ʻŌʻō during 14:00-15:00 HST on April 30. Positive change indicates tilt in the direction indicated; north component went off scale near the end of the time series (indicated by faded dashed line). Northwest-directed tilt began at about the same time as a major gravity decrease and subsequent increase. Plot covers time period indicated by gray shading in Figure 5.

The gravity signal—a decrease followed by an increase—is similar to that observed on the northeast rift zone of Mount Etna in 2002. That event was interpreted by Branca et al. (2003) as opening of a dry crack ahead of a magmatic intrusion, which caused the gravity decrease due to an overall density decrease as rock was replaced by void space, followed by filling of that crack by magma, which caused the gravity increase due to filling of the just-created void space with magma. The gravity change at Puʻu ʻŌʻō could be the result of a similar process—the decrease representing opening of a dry crack, while the increase could have resulted from filling of that crack with intruding magma. That the increase exceeded the preceding decrease might indicate that the intruding magma was denser than the agglutinated spatter, cinder, and shelly pāhoehoe that make up Puʻu ʻŌʻō's cone and surrounding lava field (Heliker et al., 2003). The crack opening and filling would not change the deformation style of the event, so the steady tilt direction despite the fluctuations in gravity (Figure 7) is also consistent with a shallow intrusion within Puʻu ʻŌʻō. The lack of any change to the crater floor at this time, as seen by webcam imagery, indicates that the lava erupted on the west flank was not sourced from within or just beneath the main part of Puʻu ʻŌʻō crater, although, as discussed below, it may have come from a lava pond on the western edge of Puʻu ʻŌʻō crater that was not visible to the webcams.

Although a conceptual model of crack opening and filling is consistent with the gravity and tilt signals, we were unable to reproduce the amplitude of the gravity signal through analytical models. Preliminary calculations based on a simple model of a dry crack to explain the observed gravity decrease require a crack geometry that does not match the field observations. For example, assuming a crack that is 1000 m high with the top close to the ground surface and matching the extent of the eruptive fissure, opening of 35 m is required to approximate the initial 200 μGal gravity decrease. If the crack is extended to the east to connect with Puʻu ʻŌʻō crater, the opening required to match the observed gravity change is still an unrealistic 13 m. A more realistic crack opening of 2 m is possible only if the dike was located directly beneath the gravity station, which clearly is not the case.

An alternative interpretation, supported by geological observations (C. Parcheta, personal communication, 2021), is that the gravity change does not reflect the opening and filling of the fissure itself, but instead multiple processes that were associated with the formation of the fissure

(Figure 8). In late April, the west side of Puʻu ʻŌʻō crater area hosted an active lava pond (Figure 8a). If the fissure intersected the crater beneath the surface, the so-called "west pond" may have drained into the fissure (Figure 8b). Two lines of evidence support this model. First, lava only erupted from the upper third of the fissure, suggesting that lava moved laterally from the west pond into the fissure, rather than rising from below. Second, there was no evidence for fountaining along the eruptive part of the fissure (Figure 2), suggesting that the lava had already degassed. In this model, the gravity decrease would be due to the drainage of the west pond, which is much closer to the observation point than the fissure and thus better able to explain the magnitude of the gravity decrease. As for the ensuing gravity increase, we speculate that a large dike was, in fact, ascending beneath Puʻu ʻŌʻō—a consequence of the weeks of pressurization of the magmatic system (Patrick et al., 2020). A dike provides the mechanisms for the formation of the fissure in the first place as well as the gravity increase, which indicates a subsurface accumulation of mass. The mass must have been significant and close to the observation point, however, to result in a gravity increase that greatly exceeded the decrease caused by draining of the west pond (Figure 8c). The gravity increase flattened after 10 minutes, indicating that the dike stalled, at least where it was close to the gravity station. Northwest-directed tilt continued to accelerate, however, suggesting that the dike might have been active to the west, far enough away from the gravimeter to be undetected by that instrument (Figure 8d). Regardless, it never breached the surface, and ultimately a barrier of some sort within the ERZ beneath Puʻu ʻŌʻō failed, leading to the lower East Rift Zone intrusion and the collapse of Puʻu ʻŌʻō crater, and removing the driving force behind the possible Puʻu ʻŌʻō dike (Figure 8e).

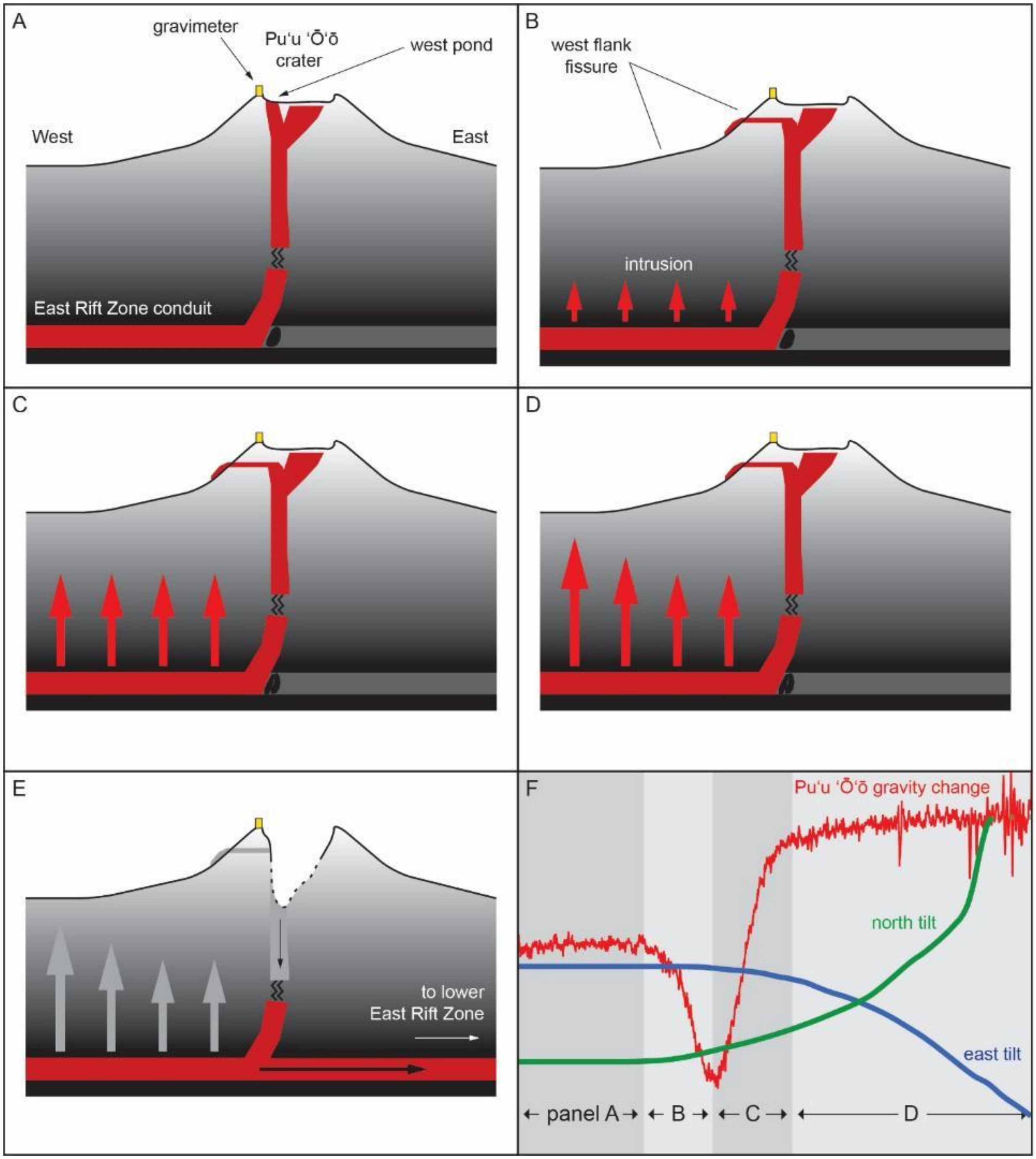

Figure 8. Schematic model (not to scale) of possible mechanism for pre-collapse gravity fluctuation at Puʻu ʻŌʻō. (A) Magma from the ERZ ascends vertically beneath Puʻu ʻŌʻō, underlying the main crater and supplying the west pond. (B) Intrusion of a dike from the ERZ opens a fissure on the west flank of Puʻu ʻŌʻō, intersecting the west side of the crater and causing the west pond to drain and erupt from the upper third of the fissure (Figure 2). This is associated with a gravity decrease measured on the crater rim of Puʻu ʻŌʻō. (C) The Dike

continues to rise beneath the cone, resulting in a gravity increase. (D) The dike stalls directly beneath the cone, causing the gravity increase to cease, but tilt continues as the dike remains active farther to the west. € a barrier of some kind beneath Puʻu ʻŌʻō ruptures, allowing magma in the ERZ to flow downrift and causing Puʻu ʻŌʻō crater to collapse. (E) Tilt and gravity change measured at Puʻu ʻŌʻō, with the time periods of the various model elements indicated.

Unfortunately, there are no data for constraining these models, which are obvious simplifications of a process that must have been exceedingly complex. Discrete earthquakes were not located during the hour before crater collapse at Puʻu ʻŌʻō, but this is not uncommon when dike intrusions result in the formation of new eruptive vents in that area; increases in tremor are the dominant seismic manifestation (e.g., Orr et al., 2015). Weather during the event was poor, so webcam views of the crater were frequently obscured and small changes in the crater might have been missed. The west pond was out of view of the main webcam, and an untelemetered research camera with a view of west pond was destroyed in the collapse of Puʻu ʻŌʻō. While there is no way to be certain of the exact nature of subsurface processes that preceded the onset of collapse at Puʻu ʻŌʻō, we suspect that some combination of the processes outlined above played a role. The formation and filling of void space in association with mass changes was almost certainly a factor, and the sources of mass change were related, directly or indirectly, to the fissure on the west flank of the cone. These events preceded both the collapse of Puʻu ʻŌʻō crater and the formation of the lower ERZ intrusion, and were thus the first events of the 2018 eruptive sequence.

5.0 Discussion

5.1 Onset of Kīlauea's 2018 lower East Rift Zone activity

Kīlauea's 2018 flank eruption and summit collapse was preceded by weeks-long pressurization of the magmatic system, initially at Puʻu ʻŌʻō and then at the summit, resulting from a decrease in lava effusion from Puʻu ʻŌʻō and causing a backup in Kīlauea's magma plumbing system (Patrick et al., 2020). This condition suggested that a change in the long-term ERZ eruption was imminent, probably involving the formation of a new eruptive vent near Puʻu ʻŌʻō as had occurred several times previously in result to similar phases of pressurization (e.g., Orr et al., 2015). By late April 2018, Kīlauea was thus poised for a magmatic event of some kind, and the lower ERZ might have been primed by long-term flank instability, which favors ERZ opening (Montgomery-Brown et al., 2020; Patrick et al., 2020). The immediate precursors of the 2018 sequence, however, are not well understood and one of the main questions is: what event started the sequence on April 30 that ultimately led to the lower ERZ eruption and summit collapse?

The eruptive fissure on the west flank of Puʻu ʻŌʻō (Figure 2) was not recognized until after the onset of the lower ERZ intrusion, and so the timing of its formation was uncertain. Based on the change in tilt that preceded the collapse of the crater floor at Puʻu ʻŌʻō (Figure 7), the fissure was suspected as having formed before the start of magma withdrawal from beneath Puʻu ʻŌʻō and the onset of the lower ERZ intrusion. Gravity data provide convincing additional evidence that the fissure was the initial event of the sequence that eventually led to the lower ERZ intrusion, starting approximately one hour beforehand. Further, the gravity data offer better resolution of the changes associated with the small eruptive fissure compared to tilt, GPS, and seismic data. Ground tilt was in the same direction with a quasi-exponential increase in rate over the course of about 45 minutes, whereas the gravity data have more structure—a major decrease followed by a larger increase, all in less than 20 minutes (Figure 7)—which we interpret as involving the formation and filling of void space (e.g., Branca et al., 2003) and possibly the formation of a dike intrusion beneath Puʻu ʻŌʻō that did not breach the surface (Figure 8). All of this occurred prior to collapse of the crater floor at Puʻu ʻŌʻō. Had they been analyzed in near real time, the gravity and tilt combination might have informed a more robust interpretation of what was happening at Puʻu ʻŌʻō, especially given that the vent area was shrouded in fog, obscuring visual observations and camera views.

The constraints from gravity and tilt indicate that the 2018 lower ERZ eruption and summit collapse started with the relatively minor eruption of a small amount of degassed magma on the west flank of Puʻu ʻŌʻō. Such an event was forecast by the Hawaiian Volcano Observatory as a likely outcome of the March-April 2018 pressurization of the magmatic system from Puʻu ʻŌʻō to the summit (Patrick et al., 2020). Lava flows from the fissure were minor, suggesting that the eruption was brief, and the lack of any evidence of fountaining along the fissure indicates that the lava was largely degassed. The overall change in tilt and gravity, and the formation of the fissure itself, suggest that a larger dike might have been rising from depth, contributing stresses that formed the fissure at the surface. If correct, this dike must ultimately have stalled without breaching the surface and relieving the accumulated pressure. Soon after the fissure's formation, a barrier to downrift flow ruptured within the core of the ERZ beneath the general region of Puʻu ʻŌʻō, leading to the lower ERZ intrusion and, a few days later, eruption (Neal et al., 2019; Patrick et al., 2020).

5.2 Lava density measurements

Continuous gravity data from Kīlauea have characterized the density of the summit lava lake at various times (Carbone et al., 2013; Poland and Carbone, 2016), and the 2018 summit lava lake withdrawal provided one final opportunity to assess that parameter. The 2018 calculation may be the most accurate to date, given the available detail of the summit vent geometry and corresponding model (Figure 4). The density obtained from the 2018 lava lake withdrawal—1700 kg m^{-3}—is greater than that from the 2011 withdrawal (950 kg m^{-3}) and 2011-2015 time series (1000-1500 kg m^{-3}). Was the lava lake getting denser with time? Or does the spread in density reflect uncertainty in the modeling?

Available evidence favors that the density of the summit lava lake did increase over time. Bagnardi et al. (2014) measured a gravity increase at Kīlauea's summit using campaign measurements collected during 2009–2012, but this increase was not accompanied by the magnitude of summit inflation that would be expected if the gravity change was due to magma accumulation alone. Instead, they interpreted the gravity data as indicative of densification of shallow magma as it degassed via the summit lava lake.

In addition, Patrick et al. (2019a) noted that the relation between changes in lava level and summit elevation varied over time. A comparison of vertical displacement from the GNSS station collocated with the summit gravimeter (Figure 1) and the elevation of the lava lake indicates that, during 2010–2013, each centimeter of uplift was accompanied by 13.1 m of lava lake rise. This ratio flattened by September 2013, and by late 2016 had became negative—

meaning that the lava level dropped even while the summit uplifted (Patrick et al., 2019a). The change in this ratio over time can be explained by an increase in the density of the summit lava column. Patrick et al. (2015) demonstrated that the lava lake was an excellent indicator of magma pressure—essentially a piezometer—and that magma reservoir pressure P could be defined by $P=\rho gh$, where ρ is the density of the summit lava column, g is the acceleration due to gravity, and h is the distance between the magma reservoir and the lava lake surface. Assuming a reservoir depth of 1500 m beneath the summit (Anderson et al., 2019), a density of 1000 kg m^{-3}, and a gravitational acceleration of 9.8 m s^{-2}, a lava level increase of 1 m implies a reservoir pressure increase of 0.01 MPa (Patrick et al., 2015). The same pressure increase can be explained by a density increase of 1 kg m^{-3} without a chance in lava level. Starting in 2013, uplift dominated at the summit, indicating that reservoir magma pressure was increasing, yet the lava level did not experience a corresponding increase (Patrick et al., 2019a)—a discrepancy that suggests the density of the lava column was increasing over time. The summit lava lake did, indeed, act as a piezometer, but changes in the density of the lava column must be accounted for in calculations of magma pressure, given that pressure is a function of both density and lava lake elevation.

The density of lava within Puʻu ʻŌʻō crater had never before been determined. It had long been assumed that the density of Puʻu ʻŌʻō lava was greater than that of the summit lava lake, since lava erupted from and near Puʻu ʻŌʻō had pre-eruptively degassed at the summit—a hypothesis first put forward by Gerlach and Graeber (1985) prior to the time of simultaneous summit and rift zone eruptions and then confirmed by the measurements of Elias and Sutton (2012). Modeling results from continuous gravity reported here support this hypothesis. Patrick et al. (2015) pointed out that during ERZ eruption pauses, the summit and ERZ vents are in magmastatic equilibrium, and there would be little magma flow along the ERZ. As a result, any difference in the elevation of the lava surfaces at the two vents would be due to lava density differences. In mid-2012, during an ERZ eruptive pause, the summit lava lake was at an elevation of 922 m, and the lava level at Puʻu ʻŌʻō was 80 m lower. This indicates that the lava column at Puʻu ʻŌʻō was slightly denser, by 50–140 kg m^{-3} (accounting for various possible summit lava lake densities). Our modeling of gravity data indicates that the lava density at Puʻu ʻŌʻō was 100–200 kg m^{-3} greater than that at the summit, consistent with the calculations of

Patrick et al. (2015). Gravity data from the two eruptive vents on Kīlauea thus confirms that density plays a major role in determining the hydraulic relation between summit and ERZ eruptive activity.

5.3 Continuous gravity as a monitoring tool

Results from Kīlauea's 2018 eruptive activity serve to emphasize the importance of gravimetry for monitoring volcanic activity. Campaign results have shown value as an early indicator of magmatic resurgence—for example, an increase in gravity preceded the onset of inflation at Kīlauea following the end of the 2018 activity (Poland at al., 2019). Continuous gravity have similar utility (Carbone et al., 2017), with sensitivity to processes that occur on relatively short timescales, like magmatic intrusions (Branca et al., 2003), volatile accumulation (Carbone et al., 2015), and magma convection (Carbone and Poland, 2012).

In 2018, continuous gravity provided, in retrospect, one of the first and most obvious indications that a change in eruptive activity was underway, with a 200 μGal gravity decrease occurring over 8 minutes, followed by a 400 μGal increase in the subsequent 10 minutes (Figure 7). Tilt changes at about the same time also indicated that a transient process was underway, but the magnitude and style of the gravity signal were readily interpretable as a magmatic event occurring in close proximity to the sensor. These data were only downloaded hourly by the Hawaiian Volcano Observatory and were not one of the data streams used to trigger an alarm, so data analysis was retrospective. Incorporating continuous gravity into other real- and near-real-time data streams, like tilt and seismic, would allow for a more robust interpretation of any anomalous activity.

Continuous gravity is not a panacea, of course. It is clear that proximity of the sensor to the source is of vital importance—a gravimeter located off Puʻu ʻŌʻō cone might not have seen the signal associated with the fissure on the west flank of the cone, for example. This principle is underscored by a temporary deployment of a continuous gravimeter during the 2018 lower ERZ eruption. For three separate ~24-hour periods in June and July, the gravimeter from Puʻu ʻŌʻō (removed in early June) was redeployed temporarily near the site of Fissure 9 (Figure 1), about

600 m uprift of Fissure 8, which was the dominant vent for the lower ERZ eruption (Neal et al., 2019). The gravimeter was operational during multiple eruptive surges prompted by summit collapse events, reflecting changes in mass flux within the magmatic conduit feeding Fissure 8 (Patrick et al., 2019c). Despite the fact that the conduit must have been within a few hundred meters beneath the surface at the location of the instrument, changes in gravity were never resolved at the Fissure 9 measurement site. The gravimeter was either too far from the source of mass change, or the changes were not of sufficient magnitude to be resolvable.

6.0 Conclusions

Continuous gravity monitoring, combined with geophysical, petrologic, and observational datasets, shed new light on several aspects of Kīlauea's eruptive activity, both in 2018 and preceding years:

(1) The gravity decrease during withdrawal of the summit lava lake in early May, combined with a detailed three-dimensional model of the summit eruptive vent, yielded a density of 1700 kg m^{-3} for the upper ~200 m of the lava lake. This is higher than has been recorded at previous times and might reflect that the lava lake density gradually increased over its lifetime owing to degassing, but it is still much less than the typical density of solidified basalt and is a testament to the presence of exsolved volatiles within the lava lake. An increase in lava-lake density over time explains why summit uplift was not accompanied by strong increases in lava-lake level after 2013, given that increases in magma reservoir pressure could be accommodated by an increase in lava level and/or the density of the lava column.

(2) Even though the evolution of crater floor collapse at Puʻu ʻŌʻō was not known in detail, the gravity record, plus a model of the vent geometry, indicate that at least 11 x 10^6 m^3 of lava drained from Puʻu ʻŌʻō and into the rift zone system below the cone over the course of two hours, and the density of that material was 1800–1900 kg m^{-3}—information that would not have been possible without continuous gravity monitoring. The greater density of the lava column at Puʻu ʻŌʻō compared to the summit is consistent with the

elevation difference of lava surfaces at the two vents and also pre-eruptive degassing at the summit.

(3) The continuous gravity record at Puʻu ʻŌʻō supports the hypothesis that the first event of the 2018 sequence was the formation of a fissure on the west flank of Puʻu ʻŌʻō cone, which involved the formation and filling (by magma) of void space and possibly the intrusion of a dike beneath the cone.

We are hopeful that these results, which emphasize the value of continuous gravity in volcano monitoring, will motivate the installation of gravimeters on additional volcanoes worldwide, especially as technological advances result in less expensive and more accurate instrumentation (Middlemiss et al., 2016, 2017; Ménoret et al., 2018; Carbone et al., 2020).

Acknowledgments

We are grateful to the staff of the Hawaiian Volcano Observatory, and especially the technical expertise of Kevan Kamibayashi, Steven Fuke, CJ Moniz, Frank Younger, Loren Antolik, and Asta Miklius, for their support of continuous gravity measurements at Kīlauea. Carolyn Parcheta provided invaluable insight into the timing of collapse at Puʻu ʻŌʻō and the characteristics of the west fissure, including her conceptual model of the involvement of the west pond. David Okita, sexpert piloting skills were invaluable to safely installing and recovering the gravimeter at Puʻu ʻŌʻō. All of the data described in this report were collected within Hawaiʻi Volcanoes National Park, and we are grateful for the collaboration and support of numerous Hawaiʻi Volcanoes National Park staff over the years in facilitating our gravity monitoring and research efforts. GNSS data are archived at UNAVCO, and gravity data are available from Poland (2020). Dan Dzurisin offered valuable input to the manuscript, and comments from Tina Neal and an anonymous reviewer greatly improved the manuscript.

References

Anderson, K.R., Johanson, I.A., Patrick, M.R., Mengyang, G., Segall, P., Poland, M.P., Montgomery-Brown, E.K., Miklius, A., 2019. Magma reservoir failure and the onset of caldera collapse at Kīlauea Volcano in 2018. Science 366, eaaz1822, https://doi.org/10.1126/science.aaz1822.

Bagnardi, M., Poland, M.P., Carbone, D., Baker, S., Battaglia, M., Amelung, F., 2014. Gravity changes and deformation at Kīlauea Volcano, Hawaii, associated with summit eruptive activity, 2009–2012. J. Geophys. Res. 119, 7288–7305, https://doi.org/10.1002/2014JB011506.

Branca, S., Carbone, D., Greco, F., 2003. Intrusive mechanism of the 2002 NE-Rift eruption at Mt. Etna (Italy) inferred through continuous microgravity data and volcanological evidences. Geophysical Research Letters 30, https://doi.org/10.1029/2003GL018250.

Carbone, D., Poland, M.P., 2012. Gravity fluctuations induced by magma convection at Kīlauea Volcano, Hawaiʻi. Geology 40, 803-806, https://doi.org/10.1130/G33060.1 .

Carbone, D., Poland, M.P., Patrick, M.R., Orr, T.R., 2013. Continuous gravity measurements reveal a low-density lava lake at Kīlauea Volcano, Hawaiʻi. Earth Planet. Sci. Lett. 376, 178-185, https://doi.org/10.1016/j.epsl.2013.06.024.

Carbone, D., Zuccarello, L., Messina, A., Scollo, S., Rymer, H., 2015. Balancing bulk gas accumulation and gas output before and during lava fountaining episodes at Mt. Etna. Sci. Rep. 5, 18049. https://doi.org/10.1038/srep18049.

Carbone, D., Poland, M.P., Diament, M., Greco, F., 2017. The added value of time-variable microgravimetry to the understanding of how volcanoes work. Earth-Science Reviews 169, 146-179, https://doi.org/10.1016/j.earscirev.2017.04.014.

Carbone D., Antoni-Micollier L., Hammond G., de Zeeuw - van Dalfsen E., Rivalta E., Bonadonna C., Messina A., Lautier-Gaud J., Toland K., Koymans M., Anastasiou K., Bramsiepe S., Cannavò F., Contrafatto D., Frischknecht C., Greco F., Marocco G., Middlemiss R., Ménoret V., Noack A., Passarelli L., Paul D., Prasad A., Siligato G. and Vermeulen P., 2020. The NEWTON-g Gravity Imager: Toward New Paradigms for Terrain Gravimetry. Front. Earth Sci., 8, 573396, https://doi.org/10.3389/feart.2020.573396

Dietterich, H.R., Diefenbach, A., Soule, A., Zoeller, M., Patrick, M.R., Major, J.J., and Lundgren, P.R., in review, Lava effusion rate evolution and erupted volume during the 2018 Kīlauea lower East Rift Zone eruption, Bulletin of Volcanology.

Elias, T., and Sutton, A.J., 2012, Sulfur dioxide emission rates from Kīlauea Volcano, Hawaiʻi, 2007–2010. U.S. Geological Survey Open-File Report 2012-1107, 25 p., http://pubs.usgs.gov/of/2012/1107/.

Gansecki, C., Lee, R.L., Shea, T., Lundblad, S.P., Hon, K., Parcheta, C., 2019. The tangled tale of Kīlauea's 2018 eruption as told by geochemical monitoring. Science 366, eaaz0147, https://doi.org/10.1126/science.aaz0147.

Gerlach, T.M., and Graeber, E.J., 1985. Volatile budget of Kīlauea volcano. Nature 313, 273–277, https://doi.org/10.1038/313273a0.

Heliker, C., Kauahikaua, J., Sherrod, D.R., Lisowski, M., Cervelli, P., 2003. The rise and fall of Puʻu ʻŌʻō cone, 1983-2002, in: Heliker, C., Swanson, D.A., Takahashi, T.J. (Eds.), The Puʻu ʻŌʻō-Kūpaianaha Eruption of Kīlauea Volcano, Hawaiʻi: The First 20 Years, United States Geological Survey Professional Paper 1676, pp. 29–51.

Johnson, D.J., Eggers, A.A., Bagnardi, M., Battaglia, A., Poland, M.P., and Miklius, A., 2010. Shallow magma accumulation at Kīlauea Volcano, Hawaiʻi, revealed by microgravity surveys. Geology 38, 1139–1142, https://doi.org/10.1130/G31323.1.

Kundu, B., Yadav, R.K., Bürgmann, R., Wang, K., Panda, D., Gahalaut, V.K., 2020. Triggering relationships between magmatic and faulting processes in the May 2018 eruptive sequence at Kīlauea volcano, Hawaii. Geophysical Journal International 222, 461-473, https://doi.org/10.1093/gji/ggaa178.

Lundgren, P., Poland, M., Miklius, A., Orr, T., Yun, S.-H., Fielding, E., Liu, Z., Tanaka, A., Szeliga, W., Hensley, S., Owen, S., 2013. Evolution of dike opening during the March 2011 Kamoamoa fissure eruption, Kīlauea Volcano, Hawaiʻi. J. Geophys. Res. 118, 897-914, https://doi.org/10.1002/jgrb.50108.

Middlemiss, R.P., Samarelli, A., Paul, D.J., Hough, J., Rowan, S., Hammond, G.D., 2016. Measurement of the Earth tides with a MEMS gravimeter. Nature 531, 614-617, https://doi.org/10.1038/nature17397.

Middlemiss, R.P., Bramsiepe, S.G., Douglas, R., Hough, J., Paul, D.J., Rowan, S., Hammond, G.D., 2017. Field Tests of a Portable MEMS Gravimeter. Sensors (Basel) 17, 2571, https://doi.org/10.3390/s17112571.

Montgomery-Brown, E.K. and Miklius, A., 2020. Periodic dike intrusions at Kīlauea volcano, Hawaiʻi. Geology, https://doi.org/10.1130/G47970.1.

Neal, C.A., Brantley, S.R., Antolik, L., Babb, J., Burgess, M., Calles, K., Cappos, M., Chang, J.C., Conway, S., Desmither, L., Dotray, P., Elias, T., Fukunaga, P., Fuke, S., Johanson, I.A., Kamibayashi, K., Kauahikaua, J., Lee, R.L., Pekalib, S., Miklius, A., Million, W., Moniz, C.J., Nadeau, P.A., Okubo, P., Parcheta, C., Patrick, M.R., Shiro, B., Swanson, D.A., Tollett, W., Trusdell, F., Younger, E.F., Zoeller, M.H., Montgomery-Brown, E.K., Anderson, K.R., Poland, M.P., Ball, J., Bard, J., Coombs, M., Dietterich, H.R., Kern, C., Thelen, W.A., Cervelli, P.F., Orr, T., Houghton, B.F., Gansecki, C., Hazlett, R., Lundgren, P., Diefenbach, A.K., Lerner, A.H., Waite, G., Kelly, P., Clor, L., Werner, C., Mulliken, K., Fisher, G., 2019. The 2018 rift eruption and summit collapse of Kīlauea Volcano. Science 363, 367-374, https://doi.org/10.1126/science.aav7046 .

Patrick, M.R., 2020. Crater geometry data for Puʻu ʻŌʻō, on Kīlauea Volcano's East Rift Zone, in May 2018. U.S. Geological Survey data release, https://doi.org/10.5066/P99QB29I.

Patrick, M.R., Anderson, K.R., Poland, M.P., Orr, T.R., Swanson, D.A., 2015. Lava lake level as a gauge of magma reservoir pressure and eruptive hazard. Geology 43, 831-834, https://doi.org/10.1130/G36896.1.

Patrick, M., Swanson, D., Orr, T., 2019a. A review of controls on lava lake level: insights from Halemaʻumaʻu Crater, Kīlauea Volcano. Bull. Volcanol. 81, 13, https://doi.org/10.1007/s00445-019-1268-y.

Patrick, M.R., Younger, E.F., and Tollett, W., 2019b, Lava level and crater geometry data during the 2018 lava lake draining at Kīlauea Volcano, Hawaii. U.S. Geological Survey data release, https://doi.org/10.5066/P9MJY24N.

Patrick, M.R., Dietterich, H.R., Lyons, J.J., Diefenbach, A.K., Parcheta, C., Anderson, K.R., Namiki, A., Sumita, I., Shiro, B., Kauahikaua, J.P., 2019c. Cyclic lava effusion during the 2018 eruption of Kīlauea Volcano. Science 366, eaay9070, https://doi.org/10.1126/science.aay9070.

Patrick, M.R., Houghton, B., Anderson, K.R., Poland, M.P., Montgomery-Brown, E.K., Johanson, I.A., Thelen, W.A., Elias, T., 2020, The cascading origin of the 2018 Kīlauea eruption and implications for future forecasting. Nature Communications 11, 5646, https://doi.org/10.1038/s41467-020-19190-1.

Poland, M.P., 2020, Continuous gravity data from Kīlauea Volcano, Hawaiʻi. U.S. Geological Survey data release, https://doi.org/10.5066/P9PP5LX1.

Poland, M.P., Carbone, D., 2016. Insights into shallow magmatic processes at Kīlauea Volcano, Hawaiʻi, from a multi-year continuous gravity time series. Journal of Geophysical Research: Solid Earth 121, 5477-5492, https://doi.org/10.1002/2016JB013057.

Poland, M.P., Carbone, D., 2018. Continuous gravity and tilt reveal anomalous pressure and density changes associated with gas pistoning within the summit lava lake of Kīlauea Volcano, Hawaiʻi. Geophysical Research Letters 45, 2319–2327, https://doi.org/10.1002/2017GL076936.

Poland, M., Orr, T.R., Kauahikaua, J.P., Brantley, S.R., Babb, J.L., Patrick, M.R., Neal, C.A., Anderson, K.R., Antolik, L., Burgess, M., Elias, T., Fuke, S., Fukunaga, P., Johanson, I.A., Kagimoto, M., Kamibayashi, K., Lee, L., Miklius, A., Million, W., Moniz, C., Okubo, P.G., Sutton, A.J., Takahashi, T.J., Thelen, W.A., Tollett, W., Trusdell, F.A., 2016. The 2014–2015 Pāhoa lava flow crisis at Kīlauea Volcano, Hawai'i: Disaster avoided and lessons learned. GSA Today 26, 4-10, https://doi.org/10.1130/GSATG262A.1.

Poland, M.P., Zeeuw-van Dalfsen, E., Bagnardi, M., Johanson, I.A., 2019. Post-collapse gravity increase at the summit of Kīlauea Volcano, Hawaiʻi. Geophysical Research Letters 46, 14430-14439, https://doi.org/10.1029/2019GL084901.

Segall, P., Anderson, K.R., Johanson, I., Miklius, A., 2019. Mechanics of inflationary deformation during caldera collapse: Evidence from the 2018 Kīlauea eruption. Geophysical Research Letters 46, 11782-11789, https://doi.org/10.1029/2019GL084689.

Segall, P., Anderson, K.R., Pulvirenti, F., Wang, T., Johanson, I., 2020. Caldera Collapse Geometry Revealed by Near-Field GPS Displacements at Kīlauea Volcano in 2018. Geophysical Research Letters 47, e2020GL088867, https://doi.org/10.1029/2020GL088867.

Wenzel, H.G., 1996. The nanogal software: Data processing package Eterna 3.30. Bull. Inform. Marées Terrestres 124, 9425–9439.